Studying the mechanism of biodiesel acting as an environmental stress cracking agent with polyethylenes

A.K. Saad[a], H.A. Abdulhussain[a], F.P.C. Gomes[b], J. Vlachopoulos[a], M.R. Thompson[a,*]

[a] *CAPPA-D/MMRI, Department of Chemical Engineering,*

McMaster University, Hamilton, Ontario, Canada

[b] *LABPOL, Department of Materials Engineering,*

Universidade Federal do Rio Grande do Norte, Natal, RN, Brazil

Submitted to: Polymer

November 2019

* Author to whom correspondence should be addressed.

Tel: (905) 525-9140 x 23213

mthomps@mcmaster.ca

Declarations of interest: The authors declare no conflict of interest.

Abstract

This paper focuses on understanding the compatibility of biodiesel with different grades of polyethylene, specifically examining the environmental stress cracking ability of biodiesel. Traditional testing methods were coupled with a nondestructive ultrasonic testing method to investigate the modes of interaction by biodiesel with the polymer. The mechanism of failure was studied by gravimetric analysis and infrared spectroscopy to monitor fluid absorption in the notched and bent specimens while attenuation in the higher harmonics of an emitted acoustic pulse followed internal stresses. The ultrasonic technique offered a unique opportunity to link fuel penetration with microstructural changes prior to visible fracturing. Analysis of the mechanism was aided by the color of the fuel showing that cracking was preceded by highly localized absorption around the notch of the specimen, whereas resin grades with apparent immunity to cracking experienced uniform absorption over the whole body of a specimen.

Keywords: Compatibility; Ultrasonic Testing; Biodiesel.

1. INTRODUCTION

The relatively inert nature, along with other valuable properties, of polyethylene (PE) have without a doubt made it a prevalent material in today's world, with uses in numerous applications ranging from simple household items, such as recycling bins, to industrial applications such as the storage of chemicals including fuel tanks in automobiles, marine vessels, and agricultural machinery [1]. As a result of its broad use, parts fabricated from PE are often exposed to aggressive environments that may cause chemical and physical changes leading to early failure if not properly selected for the use. Nearly 70 years ago, environmental stress cracking (ESC) was first identified in the polymer industry as a significant problem to be considered when selecting PE grades, especially for contact applications with fluids such as piping and tank fabrication [2-7]. An estimated 15-40% of all plastic component failures based on application can be traced to ESC [7,8]. Interestingly, the mechanism of ESC is still not completely understood despite the length of time since it was first recognized.

ESC relates to an accelerated brittle failure of a polymer, resulting from low-to-moderate stresses while in contact with fluids such as alcohols or detergents [9-16]. It is considered a physical phenomenon since the polymer chains are not chemically altered [17]. Failures related to ESC are believed to occur under highly localized conditions related to chain morphology, absorbed concentration of the contacting fluid, and concentrated stresses producing this deleterious outcome. Several testing methods are available to characterize slow crack growth (SCG) and ESC, including the standardized full-notch creep test (FNCT) (ISO 16770) [18], the notched constant tensile load test (NCTL) (ASTM D5397) [19], the Pennsylvania Notch Test (PENT) (ASTM F1473) [20], and the Bell Test (ASTM D1693) [21]. Ironically, the active fluids related to ESC often have little perceived influence on the polymer, which makes the phenomena

all the more troubling to identify. The present study arose from concerns that biodiesel could be one such active fluid.

The depletion of fossil fuel reserves along with the environmental issues associated with using them has renewed interest in biodiesel as a substitute, making its application with PE to be an immediate compatibility concern when considering that many tanks are nowadays fabricated with this material [22]. Few studies of biodiesel with PE have been conducted to date [12,23-29], finding little to no evidence that chemical interactions occur. In the face of some troubling early failures being reported to industry for parts contacting this biofuel, it seemed prudent to consider ESC as a likely cause. This is a new consideration for the polymer industry, with only two very recent studies to suggest that biodiesel could be an ESC agent [11,30]. The study by Schilling and Böhning [11] used detergents as characteristic model fluids for biodiesel and diesel to characterize ESC of different high density polyethylenes by the two mediums. Their results showed the ESC ability of biodiesel through accelerated failure in comparison to air, but with lower aggressiveness than diesel. The lower ESC effect of biodiesel had been attributed to the slower absorption rate and lower final equilibrium concentration of biodiesel in PE. In our own studies examining biodiesel as a plasticizer for PE [30], a newly developed non-destructive characterization based on nonlinear ultrasonics for monitoring internal stresses [31] noted interactions resembling those found with other popular ESC-active fluids like IGEPAL rather than commonly recognized plasticizers like toluene. The ultrasonic characterization tool has been utilized again in the present work to better understand the ESC mechanism of biodiesel with PE. In that earlier study [30], the yellowish hue of biodiesel made it possible to detect its distribution in a contacting polymer, unlike colorless traditional ESC agents like IGEPAL, leading to the hypothesis that a deeper study of the mechanism for ESC would be possible with this fluid.

Therefore, the current study conducts further research into biodiesel as an ESC agent with PEs and based on its findings, proposes a mechanism of interaction. The work uses the aforementioned nonlinear ultrasonic characterization method in conjunction with gravimetric analyses to monitor the time dependent progression of biodiesel into different grades of PE without specimen destruction at each interval of sampling. The results are meant to aid our previous study in improving material compatibility libraries for parts design involving exposure of PE to this new biofuel.

2. MATERIALS AND METHODS

2.1. Materials

Four grades of high density polyethylene (HDPE) covering a wide range of properties were used, chosen based on their differing stress cracking nature. The materials were provided by Imperial Oil Ltd (Sarnia, ON) in pellet form. A summary of properties can be found in Table 1, with data provided from the supplier. The properties of the polymer grade LA 080 were not provided by the supplier, and hence were found using suitable characterization methods. The polymer pellets of all grades were compression molded according to Procedure C of Annex 1 in ASTM D4703 and were machine cut into rectangular strips of dimensions 65 mm x 13 mm x 3 mm (thickness) for testing.

Biodiesel, a tallow-based methyl ester prepared from animal renderings, was generously provided by Rothsay Biodiesel Inc (Guelph, ON) in pure form (B100). The biodiesel, whose chemical structure is shown in Figure 1, was stored in a deep freezer at -40 ºC till used for testing to minimize oxidative degradation. IGEPAL® CA630 (Nonylphenoxy poly(ethyleneoxy) ethanol) was purchased from Sigma Aldrich (Mississauga, ON) for use in the Bell Test [32]. A low sulfur diesel (summer grade; Esso Ltd) was used in some testing.

2.2. Modification of the Bell Test

Specimen size dictated in the Bell Test standard (ASTM D1693) was too small to provide sufficient surface area to affix ultrasonic sensors for the intended analysis in this study. To overcome this issue, the length of the samples was modified, while maintaining all other dimensions (65 mm x 13mm x 3mm (thickness)), to allow simultaneous testing by ultrasonic analysis. The nicking jig used in the Bell Test was also modified to allow notching of the new sample sizes.

To reasonably ensure the same stresses would be concentrated at the notch of the modified samples, as in the original test, the radius of curvature (5.1 mm) for bending was preserved. Modified u-shaped holders were made to hold only one sample while maintaining the radius of curvature at 5.1 mm. This setup allowed ultrasonic testing on the samples, one at a time, without having to remove them from their holder, hence maintaining uninterrupted stresses on a specimen throughout the experiment.

Each sample was immersed in a sealed glass tube containing the aqueous solution of 10% biodiesel, unless otherwise stated, and placed in a heated circulating water bath (VWR Corporation) at 50 ºC till the sample failed or after 1000 hours of immersion time had passed. It should be noted that the oxidative degradation of biodiesel occurring from prolonged testing at 50 ºC, has not been found to affect its rate of diffusion into the polymer or the mechanical properties of the polymer relative to neat biodiesel [30]. Each tube was agitated daily to ensure proper mixing and samples were taken out at documented times during the experiment for further analysis. After each of the analyses described below, at least until failure, the sample was placed back the glass tube and returned to the water bath; a sample was removed from the solution for

no more than 20 minutes each time for analysis. The control case for the study tested HD 6908.19 in water alone at 50℃. A minimum of five samples were tested for each grade of PE.

2.3. Gravimetric analysis

The absorption of fluid into a sample was monitored gravimetrically at documented times with a Mettler Toledo AE200 Analytical Balance. The periodicity of testing was dependent on the ESCR of the polymer grade: for grade HD 6908.19, testing was done every hour; HD 6605.70 was tested every day; grades HD 8660.29 and LA 080 were tested every two days. The surface of a sample and its housing was wiped dry carefully using paper towels before weighing. The concentration of absorbed biodiesel in the samples was calculated based on percent mass gain.

2.4. Ultrasonic testing

To monitor structural changes in the PE samples due to biodiesel penetration over time, nonlinear ultrasonics analysis was used following the gravimetric analysis mentioned above. Following a similar procedure described in earlier work [31], an emitter (resonant type, R15a) and receiver (broadband type, F30a) ultrasonic sensor (Physical Acoustic Corporation) were affixed to the surface of the specimen using high vacuum grease (Dow Corning) at a center-to-center distance of approximately 30 mm. Figure 2 shows a schematic of a bent sample with the ultrasonic sensors coupled to its surface. Ultrasonic guided waves were produced in a sample by pulse transmission at frequencies from 135 to 165 kHz in 1 kHz step increments produced with an Agilent 33210A waveform generator. The received signal was amplified using a Physical Acoustic 2/4/6c amplifier set to +40dB and collected at an acquisition rate of 4 MHz using a National Instruments 10 MHz 12-bit 4-channel data acquisition system. Each signal was converted to the frequency domain by fast Fourier transform (FFT). The frequency dependent

amplitudes for all 31 spectra were averaged to get a single spectrum representing the response of a sample to the signals emitted. An ultrasonic parameter was calculated as the amplitude ratio of the third harmonic peak (A_3) over the amplitude of the primary emitted frequency ($\mathbf{A_1}$); the frequency range of this higher harmonic was selected based on previously identified guided wave modes for the specimens due to low attenuation. To minimize errors brought about by ambient noise and sample heterogeneity related to variations in crystal morphology among specimens, the whole process was repeated four times before returning a sample to the glass tube and the recorded results were averaged to attain the presented ultrasonic parameter at each time step in the ESC test.

2.5. Infrared vibrational spectroscopy

Prior to analysis, a specimen from the ESC test was gently washed with de-ionized water and wiped to remove residual biodiesel. In order to identify the depth of biodiesel diffusion at the notched region, thin cross-sectional films perpendicular to the longitudinal axis were cut from the exposed fracture plane of a specimen using a microtome (American Optical Corporation). Each film was cut with a thickness of 100 μm. The same preparation was carried out at the end of the specimen, furthest from the notch/crack. When the samples that did not fail, a specimen was microtomed while still bent, at the notch, and at the end of the specimen. Fourier-transform infrared spectroscopy (FT-IR) was performed with a Thermo Scientific Nicolet 6700 in attenuated total reflection (ATR) mode on the collected films, for a sample at the beginning of an ESC test (before immersion in biodiesel solution) and at the end of the test (after cracking in biodiesel solution or after 1000 hours of immersion). An average of 64 scans at a resolution of 0.4 cm^{-1} were reported for the mid-range wavenumbers (between 700 and 4000 cm^{-1}).

2.6. Microscopic imaging

Optical images were taken using a Keyence vhx-5000 digital microscope. 5x and 50x lenses was used to obtain high quality digital pictures of a sample. Images of crack initiation were taken when failure was first witnessed visually, whereas images of an intact notch were taken after >1000 hours immersion in the aqueous biodiesel solution.

2.7. Crystalline characterization using Differential Scanning Calorimetry

Differential Scanning Calorimetry (DSC) was used to estimate the crystallinity content for each grade tested. DSC characterization was preformed using a Q2000 DSC from TA Instruments, over a temperature range of -50 ℃ to 250 ℃ at a ramp rate of 10 ℃/min under nitrogen purge. Approximately 10 mg of each polymer grade was taken from the notched area and transferred into a Tzero non-hermetic aluminum pan. The percent crystallinity was calculated based on the measured enthalpy of the melting transition and a theoretical heat of fusion for a 100% crystalline PE (293 J/g).

3. RESULTS AND DISCUSSION

3.1. Benchmarking biodiesel as a stress cracking agent

The first studies in this work sought to confirm that biodiesel was an ESC agent for the grades of PE under investigation and to compare its aggressiveness to a known ESC agent, IGEPAL (IGEPAL CA630). In the study, samples of HD 6605.70 were tested against six different media: pure biodiesel (B100), an aqueous solution of 10% biodiesel, 10% biodiesel in petroleum diesel (B10 solution), an aqueous solution of 10% IGEPAL, water, and air. Samples in B100, B10, and the aqueous solution with 10% biodiesel cracked after 13 days, depicting comparable aggressiveness between the three mediums, while the baseline conditions in water and air cracked after prolonged testing (>30 days). Analysis of the fracture area of the samples

showed a significant decline in fibrillation at the crack with biodiesel compared to water- and air-aged samples, indicative of a less ductile failure in the presence of the biofuel. For its tests, the samples immersed in an aqueous solution with 10% IGEPAL showed cracking in less than 1 day (approximately 20 hours). The fracture area of the IGEPAL-aged samples showed a complete absence of fibrillation, exhibiting a brittle failure typical of an exclusively ESC response. Based on this comparison, considering the time to failure and the failure mode displayed with this PE grade, the nature of biodiesel was considered to share a tendency for ESC with IGEPAL, albeit with less aggressiveness.

With similar cracking aggressiveness witnessed for biodiesel by the different solvents of dilution, the remainder of testing in this study was done with the aqueous solution of 10% biodiesel. A yellow/orange coloration left in PE samples by biodiesel was much more distinct with the aqueous solution, showing preferred absorption during aging and assisting analysis of the ESC mechanism. The ESC observations with biodiesel in petroleum diesel were notably concerning from the standpoint of tank fabrication, making future studies recommended, but this solution was considered less suitable to examining the mechanism of ESC.

3.2. Monitored aging of immersed PE samples in biodiesel

Simultaneously conducted with the ultrasonic testing discussed in a later section, gravimetric analysis was used to monitor the absorption rates and final uptake concentrations of biodiesel in the different grades of PE. Figure 3 shows the percent weight gain for the four PE grades plotted against immersion time with the aqueous solution of 10% biodiesel; presenting all curves on the same graph required two timescales to be used. The presented curves represent the best fit of 3-5 repeated trials using a logarithmic function with a $R^2 > 0.9$. In all grades, the rate of absorption of biodiesel was highest initially. ESC never occurred during the period of rapid

fuel absorption by the PE samples, but rather once the rate of mass gain had slowed, and that failure times were shorter with less mass gained. The eventual decline in this absorption rate is explained in part by a thin surface film of biodiesel gradually forming to reduce the effective concentration gradient [26], but more likely attributed to the microfibrillar morphology of PE that is becoming increasing aligned due to the bending stresses. The closely packed fibrillar mass reduces sorption and decreases diffusivity locally [33]; Peterlin [34] has likened the taut polymer chains to crystals reducing the internal channels for a penetrant. The curves indicate that all grades had not fully reached equilibrium before cracking, which is when data collection was stopped; however, the trends suggest little further weight gains was expected.

The polymer grades that did not crack (specifically HD 8660.29 and half of the LA 080 samples) showed higher final percent mass gains corresponding to their higher initial absorption rates, not simply because the samples were immersed longer in the biofuel. HD 8660.29 showed a mass gain of 4.17±0.15% after not cracking, while the uncracked LA 080 samples showed a slightly lower gain of 3.78±0.51%. Correspondingly, the cracked samples witnessed lower mass gain with LA 080 (3.66±0.22%) being higher than HD 6605.70 (2.62±0.23%) and HD 6908.19 (1.65±0.26%). The control of HD 6908.19 showed negligible weight gain in water (0.24%).

One of the reasons for the differing biodiesel mass gain among the grades was their varying crystallinity. Measured at the notch by differential scanning calorimetry (DSC), the estimated crystallinity for each grade is shown in Table 2. A lower mass gain corresponded with higher crystallinity of the polymer, seen for example by comparing HD 6908.19 versus HD 8660.29. The higher crystalline content (lower amorphous content) presented a more torturous path for the absorbed biodiesel to collect in the amorphous regions of the polymer, resulting in a material with lower permeability to biodiesel [30].

The yellow/orange color of biodiesel offered an interesting opportunity to visually track the preferred areas of absorption in a bent specimen over time. PE grades exhibiting ESC cracking were darkly stained by the biodiesel, almost exclusively in the area of the fracture, while the rest of the specimen only showed a light-yellow tint (if at all). Conversely, grades that did not crack would appear yellow all over but never reach such a dark color. Visual inspection of the HD 8660.29 samples showed yellow staining over the whole body and not just at the notch. Conversely, darker yellow staining was witnessed primarily where the crack would eventually form for HD 6605.70 and HD 6908.19 samples. The grade LA 080 represented a unique case. Approximately 50% of the time, immersed samples would fail and, in those cases, the coloration was localized but otherwise the whole body exhibited yellowing. This was a fascinating general observation since it highlighted early in the test that a sample was more likely to crack at some point if the notch region got darker in color.

Figure 4 shows FT-IR spectra in the range of 1700-1800cm^{-1} of microtomed cross-sections taken at the crack/notch area (Figures 4(a) and 4(c)) and at the ends of a rectangular specimen (Figures 4(b) and 4(d)) for HD 6605.70 (failed) and HD 8660.29 (did not fail). The bottom spectrum in each plot corresponded to a blank (i.e. sample of the grade that was never immersed in solution), whereas the three spectra above corresponded to the absorbed biodiesel at the exposed surface of the samples and at 100-micron and 400-micron increments deeper. The characteristic peak showed in each spectrum at 1735-1750 cm^{-1} corresponded to the ester of biodiesel, highest in intensity at the surface of samples to highlight greatest concentration while rapidly declining in intensity in the deeper cross-sections to indicate limited penetration. The biodiesel was not filling the cracks as a trapped liquid but rather, was absorbed into the matrix near the crack surface. The results showed significant differences at a depth of 100 micron but

minimal differences deeper (looking forward to the 400-micron depth spectra in the figure). Focusing on the cross-sections at 100-micron depth in all four plots, the ends of the specimens experiences the lowest biodiesel absorption and was similar in absorbance intensity for the two grades (plots (b) and (d) in the figure). Conversely, the cross-sections at the notch showed a higher absorbance for biodiesel in both grades (plots (a) and (c) in the figure), but the absorbance intensity was much greater in the grade that cracked. These results confirm the observations of coloring in the specimens, specifically that very localized fluid absorption occurs with ESC, though the FT-IR analysis notes that the higher surface area and stresses of the notch afforded greater biodiesel absorption even when the sample did not fail.

3.3. Analysis by nonlinear ultrasonics

Over the duration of a test, bent PE samples were monitored regularly by acoustic sensors using a nonlinear ultrasonics technique. The technique is based on guided waves, providing the ability to distinguish morphological changes pertaining to inter-crystalline regions of the polymer without destructive testing. Previous investigations [30,31] have shown signal frequencies in the region of the third harmonic are correlated with structural anisotropy, which monitored over time are related to internal stresses attributed to deformation or chemical swelling. This technique shows small differences in value attributed to the crystallinity of a samples, appearing more sensitive to changing stresses when crystalline content is lower. By testing in this non-destructive manner, it was possible to return specimens to the Bell Test apparatus for further aging.

Figure 5 shows two examples of the acoustic spectral pattern pertaining to HD 6605.70, before immersion and once microcracking began in the aqueous solution with 10% biodiesel, with denoted changes in the distinct third harmonic region (A_3, between 400-500 kHz) being

highlighted. Second order and other higher order harmonic peaks were attenuated in the dispersive material and thus not used for analysis. The decline in A_3 occurred in response to changing internal stresses; these stresses are reportedly related to microstructural asymmetries and discontinuities created by penetrating fuel into the polymer [35]. In this case, the biodiesel promoted crystal slip, which decreased the internal stresses within the polymer. In comparison, conventional plasticizers producing a more ductile failure like toluene, which is not an ESC agent, have the opposite result on the amplitude of A_3, as previously reported [30]. A toluene-plasticized polyethylene exhibits an increase in the ultrasonic parameter as a result of increasing internal stresses, in that case created by swelling. As discussed below, grades showing only SCG would also show an increase in A_3 at the time of cracking, meaning that ESC and its related brittle fracture produces a distinctive response in the acoustic technique which can be monitored.

The differing internal stresses being reflected in the acoustic analysis between failures by ESC versus SCG are associated with the extent of intra-crystalline molecular connections present, such as tie molecules (TMs) or entangled cilia or loose loops. These connections traversing throughout amorphous regions hold crystallites in proximity to one another, preventing them from slipping or being cleaving under stresses which would otherwise result in macroscopic brittleness [36, 37]. Principally, in the field of ESC, one focuses on TMs as stress transmitters that connect the interlamellar crystalline regions of PE and influencers of SCG resistance [31, 38-42]. The primary assumption of this ultrasonic technique is that propagation of ultrasonic waves in PE will be dispersive and different from a perfect elastic body. Thus, the non-linear interaction of the ultrasonic vibrations with the discontinuities of a semi-crystalline network (such as those created by the penetration of solvents) will generate frequencies different from original wave introduced, which are detectable in the higher order harmonics [31, 43, 44].

316 Figure 6 plots the ultrasonic parameter, related to A_3, over time for HD 6605.70 and HD
317 6908.19, which both showed localized yellowing at the notches of their bent samples while
318 immersed in the aqueous solution of 10% biodiesel. Since these grades exhibited failures in the
319 presence of biodiesel, the point when crack initiation began was marked in the plots for
320 reference; a micrograph of the type of cracking observed is included in the figure for HD
321 6605.70. The micrographs are added to the plots to show an example of the crack that was
322 visually detected at failure relative to the undamaged notch region. Three repeats for each grade
323 are shown to highlight the consistency of the trend being observed by the acoustic technique,
324 presented on the basis of immersion time or mass absorbed; the curves relative to mass absorbed
325 offered less obvious trends compared to time, and hence are discussed later in the section after
326 more examples have been presented. Based on immersion time (Figure 6 (a, c)), there was
327 always a significant initial decrease in the ultrasonic parameter that can be related to decreases in
328 internal stresses [30]. The rate of absorbed biodiesel was always highest during this period as it
329 first contacted the fibrillated surface inside a notch (as noted in Sec. 3.2). This localized
330 absorption of the fluid at the notch, by what is presumed to be stress-enhanced diffusion into the
331 bent specimen, plasticized the polymer and reducing the load-bearing resistance of inter-
332 crystalline chains in the amorphous regions and causing a decrease in the ultrasonic parameter to
333 a minimum value. This minimum ultrasonic parameter is referred herein as the "critical
334 ultrasonic parameter value" (CUPV). For polymers prone to ESC, the decline proceeds over a
335 considerable period of time till reaching CUPV and to a much lower parameter value compared
336 to grades more prone to SCG (discussed below). The lower CUPV was assumed as a result of
337 the few TMs attributed to polymers prone to ESC to resist crystal slip in the presence of
338 deformational stresses [31, 38-42].

339 A plateau in the ultrasonic parameter follows upon reaching CUPV. For ESC-prone
340 grades, as shown in Figure 6, the plateau proceeded for a considerable period of time before the
341 parameter increased ahead of crack initiation. The plateau represents a period of rearrangement
342 for the amorphous microstructure, presumably with disentanglement of cilia retarding crystal
343 slip. This rise in the ultrasonic parameter value was related to inter-crystalline resistance, which
344 theoretically related to the few TMs being stretched. Once major cracking occurred, the
345 parameter value decreased again. At this point, the ultrasonic parameter was no longer
346 considered exclusively correlated with the elastic properties of the polymer and was now being
347 significantly affected by the physical presence of a crack. In the face of significant interference
348 to elastic wave emissions by the propagating crack [45], it was felt that this final drop in the
349 parameter value should not be related to morphological changes or the ESC mechanism.
350 To study the time-based trend in more detail, Figure 7 plots the change in the ultrasonic
351 parameter for a control, in this case HD 6908.19 immersed in water, where the fluid effects on
352 cracking should not be present. The three samples in the control appear similar to each other in
353 trend relative to immersion time. The initial decrease in the ultrasonic parameter occurred in
354 response to decreasing internal stresses due to relaxation of the sample after notching and
355 bending; the duration of the drop was approximately half of the recorded time for the same grade
356 immersed in biodiesel (Figure 6(c)). In the absence of biodiesel, the decline would have been
357 largely due to stress relaxation being under constant strain. The CUPV tended to be higher for
358 the controls compared to samples that cracked in biodiesel, but more distinctly there was a
359 negligible plateau for samples experiencing SCG rather than ESC. The following increase in the
360 ultrasonic parameter occurred in response to increasing internal stresses related to resistance in
361 the intercrystalline region against crystal slip; without biodiesel (or for grades that did not

362 experience ESC) the ultrasonic parameter always rose to positive values. The control specimens
363 cracked in a ductile manner with noticeable fibrillation just before 7 h had lapsed, resulting in the
364 final decrease in the ultrasonic parameter.

365 The results in Figures 6 and 7 are following the internal stresses in different grades of PE,
366 hypothetically related to their interlamellar regions and influenced by the penetration of
367 biodiesel. As mentioned above, the decrease in the ultrasonic parameter to the minimum value
368 (CUPV) is considered a result of the plasticization of the TMs from localized fluid absorption at
369 the notch when biodiesel was present. The plateau at CUPV indicated a point where two
370 opposing phenomena of plasticization and SCG are momentarily in balance. With less sensitivity
371 of the polymer to ESC (i.e. higher F_{50}), more biodiesel was absorbed while the duration of the
372 initial decline and plateau in the ultrasonic parameter was longer. Naturally, it was assumed these
373 durations just grew longer for grades never displaying a failure during the test, since it has
374 already been established that they absorbed a higher amount of biodiesel. In general, this
375 assumption proved true in the acoustic analysis though one should not overlook the fact that the
376 biodiesel was no longer displaying localized absorption at the notch (referring to Sec. 3.2). To
377 demonstrate the acoustic response for grades that did not fail, Figure 8 (a-d) shows the change in
378 the ultrasonic parameter for HD 8660.29 and LA 080 on both a time basis and mass gain basis
379 while immersed in the aqueous solution of 10% biodiesel; LA 080 was included in this section
380 since it sometimes did not crack and in those cases, the specimen did not show localized
381 coloration at the notch. The included micrograph in the figure shows only a notch without
382 cracking after >1000 hours of immersion. On the basis of time, the plots show the decline and
383 plateau for very long duration, with the only difference being that there was no rise in the
384 acoustic parameter at the end of the plateau. LA 080 was the peculiar case, since the two failed

samples (Samples 1 and 2) showed localized coloring of the notch and the rise in the ultrasonic parameter prior to visually seeing cracks just like HD 6605.70 and HD 6908.19. Conversely, the two samples that did not fail (Samples 3 and 4) showed trends similar to HD 8660.29.

Due to the apparent relevance of biodiesel absorption in the ESC testing, the acoustic analysis was also conducted on a mass gain basis (Figure 6(b, d) and Figure 8(b, d)). Examining the plots for grades that failed and those that did not fail, there does not appear to be an identifiable difference in the displayed trend. The time and mass basis trends for LA 080 and HD 6605.70 appeared similar, presumably showing that their failure was driven by both factors simultaneously and would be consistent with the expected mechanism for ESC. However, the mass basis trend for HD 6908.19 looked similar to the observed trend with HD 8660.29, though only the former grade showed ESC failure in the tests. The lack of a distinctive trend for ESC on a mass basis was considered to be significant due to the discovered relevance of localized absorption to the failure mechanism. The gravimetric analysis conducted was based on a bulk measurement and it is reasonably speculated that only a fraction of the total absorbed mass was relevant to cracking based on our observations in this study.

3.4. Proposed mechanism for environmental stress cracking by biodiesel

Several methodologies have been proposed to explain the precise molecular mechanism leading to ESC [2, 46-50]. Two differing theories have attempted to explain ESC. One explanation believes exposure to an ESC agent reduces the surface energy for crack formation and therefore, lowers the stresses required for failure in comparison to PE being exposed to an inert environment [16, 50]. This hypothesis may assist the ESC mechanism, but it is believed to be a minor aspect when considering the overall mechanism [16]. In the second theory, which we believe is supported by the observations of this study, consider the important aspect of the ESC

agent is not at the specimen surface but rather being absorbed as a plasticizer [50]. The basis of the proposed mechanism was founded on the hypothesis that the concentration-limited plasticization mechanism proposed by Rogers et al. [10] for ESC explained the nature of biodiesel with PE. Reflecting on IGEPAL which experiences lower absorption in PE (~0.25 wt%, found in a parallel study by the authors) and earlier failures (Table 1) than biodiesel, we see a minute amount of plasticization accelerates ESC (affecting the TMs without overall relief of building internal stresses), whereas more plasticization slows ESC (affecting the TMs but also relieving overall stresses while sufficient agent is being progressively absorbed). The following outlines key elements of Roger's plasticization mechanism as it applies to biodiesel in the Bell Test, using Figure 9 as an aid in the explanation:

1. Notched specimens show fibrillation localized to the notch tip under the initial bending stresses but prior to immersion in the biodiesel solution, as shown in Figure 9(a). Internal stresses become concentrated at the front of the notch, as shown by Phase 1 of Figure 9(b), being under constant strain in the testing apparatus.
2. Upon immersion, the biodiesel contacts the higher surface area of fibrillated mass inside the notch, being preferentially absorbed at this site of highly concentrated stresses. Studies by Hittmair and Ullman [51] have shown increased penetration of liquids into polymers experiencing increased stresses. If the contacting fluid has a plasticizing nature on the polymer, like biodiesel with PE, then the localized absorption is a means to lower the internal stresses in the material, more quickly and to a greater degree than the inherent stress relaxation behavior of the polymer. For ESC, the polymer experiences reduced inter-lamella strength by plasticization of the few TMs in the amorphous regions of the fibrils (Phase 2).

3. A critical component of Roger's mechanism is the limited effectiveness of the stress cracking agent as a plasticizer such that its effects are constrained to the amorphous regions, with negligible influence on the dimensions of the crystals. Various authors believe that this absorption must be localized to the amorphous phase [2, 46-48]. This limited plasticization allows for more rapid/extensive crystal slip under the applied bending stresses, accelerating chain extension of the few TMs present and beginning the disentanglement of cilia. The orientation of these extended chains will decrease diffusion rates, countered the primary driver in lowering the local energy state in the notch area.
4. Two opposing phenomena (internal stresses concentrating in the tie molecules at the notch versus relief of those stresses through plasticization by the penetrating biodiesel) appear on the bulk to be momentarily in equilibrium. The building internal stresses, seen by acoustic at the end of the plateau region, comes from 'weak points' caused by the non-uniform plastic deformation of a bent sample [52]. These 'weak points' can be generated chemically, thermally, and mechanically by non-uniform plastic deformation and by crazing [53, 54]. Eventually, the TMs begin to fail under these internal stresses despite plasticization, and crack propagation results (Phase 3).
5. Microscopic voids in the formed crazes coalesce and initiate a smooth crack with very little fibril generation, which extends beyond the original localized stress region of the notch. A new localized high stress region is formed at the crack tip and is plasticized by the biodiesel at the new crack tip region as Phase 2 is repeated (Phase 4). Lustiger et al. [55] have shown evidence of the formation of secondary crazes in samples undergoing ESC.
6. The process repeats as the crack continues to grow progressively, over a thin plane

normal to the applied stress, resulting in the eventual failure of the material (Phases 5 and 6).

For this mechanism to be valid, an explanation should naturally evolve from it that reasonably explains why a grade does not fail. We accept though the explanation of others that ESC resistant polymers possess a higher frequency of TMs [36, 37]. When there are many TMs to transmit stresses and so, internal stresses are slower to concentrate at the notch, there is no driver to preferentially absorb biodiesel but also a slower orientation of the TMs present. More biodiesel is ultimately absorbed without the hindrance of extensive chain orientation and in the presence of so many TM as well as plasticizing fluid, polymer crystals will yield and unravel rather than cleavage of the TMs in the presence of the continual bending stresses. The internal stresses become constant as plasticization balances the influence of bending stresses on the microstructure of the polymer. No crazing results from this scenario. LA 080 must exist at the boundaries of molecular structure and crystallization kinetics to obtain a density of tie chains sensitive enough to minor variations in solidification that gives both possible outcomes.

3.5. Interaction of biodiesel with the different grades of polyethylene

This last section gives some consideration to the differences and similarities in the environmental stress cracking resistance (ESCR) results presented in Table 1 for the standard IGEPAL detergent versus Table 2 with biodiesel, based on the grades of PE. The findings attained in this investigation show consistency between the two ESC media based on the trend in F_{50} failure times relative to the different grades, with a potential correlation between the crystalline content and the molecular weight of the polymer (crudely implied in this case by MFI). Apart from LA 080, an inverse correlation is seen between the crystalline content of the samples and their ESCR by biodiesel. Polymer grade HD 6908.19 with the highest crystalline

content (69%) and lowest molecular weight (highest MFI - 8.2 g/10 min) showed the lowest resistance to ESC by failing quicker than all the other grades after 4.73±0.40 hours by biodiesel and 3 hours with IGEPAL. The low molecular weight associated with the polymer decreased the probable formation of TMs and the high crystallinity increases the stiffness of the sample, which induced large stresses on fibrils in the notch when bent. We did note earlier that this grade might not be failing by ESC, with cracking unrelated to the environmental fluid, but since its failure time in biodiesel was greater than in water it was still considered an ESC failure in this discussion. The grade with the second lowest resistance to ESC was HD 6605.70 at 158.82±9.33 hours (20 hours with IGEPAL). Its relatively high crystallinity (58%) and low molecular weight (high MFI – 5.0 g/10 min) have made it susceptible to ESC by biodiesel but with a higher resistance than HD 6908.19. The higher molecular weight and lower crystallinity of this grade in comparison to HD 6908.19 have allowed it to last longer in biodiesel without cracking.

The grade HD 8660.29 showed the highest resistance to ESC by biodiesel by not cracking despite being immersed for >1000 hours (40 hours with IGEPAL), by having the lowest crystallinity (50%) and a relatively higher molecular weight (low MFI – 2.0 g/10 min) to the others tested. Our previous investigations [30] on this polymer grade showed increased fuel uptake and consequently a greater extent of plasticization by biodiesel with this low crystallinity/low density grade due to its larger free volume (V_f) related to amorphous content.

The correlation between resistance to ESC by biodiesel and crystallinity that was seen in the other polymers could not be seen with LA 080 and this can be attributed to its very high molecular weight (very low MFI – 0.3 g/10 min). LA 080 was found to be susceptible to both ESC and plasticization by biodiesel. The samples that cracked in biodiesel failed after 716.03±47.75 hours (47 hours with IGEPAL). It seems that the high crystallinity (61%) of this

PE grade has made some samples susceptible to ESC; while the very high molecular weight has made some samples of this grade resistant to ESC and prone to plasticization by biodiesel instead.

There are many morphological features related to molecular structure that are correlated with one another, thus making it difficult to establish firm relationships to long-term fracture resistance without seeing contradictory findings in other studies [56]. For example, some studies [57, 58] have found that decreasing spherulite sizes improve crack propagation resistance, while others [59, 60] have suggested that the spherulite size has no effect. As a result, further investigations on morphological features of PE, to better understand their effect on the failure of samples when immersed in biodiesel, are still needed.

4. CONCLUSIONS

The investigation into the compatibility of biodiesel with PE for use in fuel-contact services has revealed that the biofuel possesses both ESC and plasticization properties towards the polymer. The fatty acid methyl ester was found to be a plasticizing agent for all grades of PE but it was more of an ESC agent to some, with the different modes of interaction attributed to the crystalline content and molecular weight of the polymer.

Through the course of testing, a dark yellowing related to the biodiesel appeared to concentrate around the notched area of a bent specimen but only for PE grades that would eventually crack. This was a unique observation offered by the biofuel that highlighted previously unreported differences in the nature of sorption in ESC testing. The coloration of PE by biodiesel combined with a non-destructive acoustic analysis technique employed in the study allowed for validation of the previously reported concentration-limited plasticization mechanism for ESC.

Further studies will concentrate on investigating the morphological features of PE to better understand their effect on the failure of samples when immersed in biodiesel. Particular attention should be given to the crystal structure and how it affects fluid absorption in the area of the notch.

ACKNOWLEDGEMENTS

The authors would like to thank Imperial Oil Ltd. and the Natural Sciences and Engineering Research Council (NSERC CRDPJ 508384-2016) for funding the work. The authors would like to especially thank Ron Cooke at Imperial Oil for his advice, supply of materials, and technical insights, and Heera Maraway at the McMaster Manufacturing Research Institute (MMRI) and Vladimir Gritschine at McMaster University for their help with testing.

REFERENCES

[1] O.-G. Piringer, A.L. Baner, Plastic packaging: interactions with food and pharmaceuticals, Wiley-VCH, Weinheim, 2008.

[2] J.M. Lagarón, J.M. Pastor, B.J. Kip, Role of an active environment of use in an environmental stress crack resistance (ESCR) test in stretched polyethylene: Polymer. 40 (1999) 1629–1636. doi:10.1016/s0032-3861(98)00406-6.

[3] N. Pons, A. Bergeret, J.-C. Benezet, L. Ferry, F. Fesquet, An Environmental Stress Cracking (ESC) test to study the ageing of biopolymers and biocomposites, Polymer Testing. 30 (2011) 310–317. doi:10.1016/j.polymertesting.2010.11.015.

[4] A. Ward, X. Lu, Y. Huang, N. Brown, The mechanism of slow crack growth in polyethylene by an environmental stress cracking agent, Polymer. 32 (1991) 2172–2178. doi:10.1016/0032-3861(91)90043-i.

[5] J.J. Cheng, M.A. Polak, A. Penlidis, Influence of micromolecular structure on environmental stress cracking resistance of high density polyethylene, Tunnelling and Underground Space Technology. 26 (2011) 582–593. doi:10.1016/j.tust.2011.02.003.

[6] A. Ghanbari-Siahkali, P. Kingshott, D.W. Breiby, L. Arleth, C.K. Kjellander, K. Almdal, Investigating the role of anionic surfactant and polymer morphology on the environmental stress cracking (ESC) of high-density polyethylene, Polymer Degradation and Stability. 89 (2005) 442–453. doi:10.1016/j.polymdegradstab.2005.01.023.

[7] D.C. Wright, Environmental stress cracking of plastics, Rapra Technology, Shrewsbury, 1996.

[8] Arnold, J. C. "Environmental stress crack initiation in glassy polymers." *Trends in polymer science* 4.12 (1996): 403-408.

567 [9] R.A. Isaksen, S. Newman, R.J. Clark, Mechanism of environmental stress cracking in linear
568 polyethylene, Journal of Applied Polymer Science. 7 (1963) 515–531.
569 doi:10.1002/app.1963.070070210.
570 [10] K. Tonyali, C.E. Rogers, H.R. Brown, Stress-cracking of polyethylene in organic liquids,
571 Polymer. 28 (1987) 1472–1477. doi:10.1016/0032-3861(87)90344-2.
572 [11] M. Schilling, M. Böhning, H. Oehler, I. Alig, U. Niebergall, Environmental stress cracking
573 of polyethylene high density (PE-HD) induced by liquid media - Validation and verification of
574 the full-notch creep test (FNCT), Materialwissenschaft Und Werkstofftechnik. 48 (2017) 846–
575 854. doi:10.1002/mawe.201700065.
576 [12] M. Schilling, U. Niebergall, I. Alig, H. Oehler, D. Lellinger, D. Meinel, et al., Crack
577 propagation in PE-HD induced by environmental stress cracking (ESC) analyzed by several
578 imaging techniques, Polymer Testing. 70 (2018) 544–555.
579 doi:10.1016/j.polymertesting.2018.08.014.
580 [13] P. Sardashti, A.J. Scott, C. Tzoganakis, M.A. Polak, A. Penlidis, Effect of Temperature on
581 Environmental Stress Cracking Resistance and Crystal Structure of Polyethylene, Journal of
582 Macromolecular Science, Part A. 51 (2014) 189–202. doi:10.1080/10601325.2014.871934.
583 [14] A. Adib, C. Domínguez, J. Rodríguez, C. Martín, R.A. García, The effect of microstructure
584 on the slow crack growth resistance in polyethylene resins, Polymer Engineering & Science. 55
585 (2014) 1018–1023. doi:10.1002/pen.23970.
586 [15] M. Schilling, U. Niebergall, M. Böhning, Full notch creep test (FNCT) of PE-HD –
587 Characterization and differentiation of brittle and ductile fracture behavior during environmental
588 stress cracking (ESC), Polymer Testing. 64 (2017) 156–166.
589 doi:10.1016/j.polymertesting.2017.09.043.

590 [16] L.M. Robeson, Environmental stress cracking: A review, Polymer Engineering & Science.
591 53 (2012) 453–467. doi:10.1002/pen.23284.
592 [17] Soares, João BP, R. F. Abbott, and J. D. Kim. "Environmental stress cracking resistance of
593 polyethylene: The use of CRYSTAF and SEC to establish structure–property
594 relationships." *Journal of Polymer Science Part B: Polymer Physics* 38.10 (2000): 1267-1275.
595 [18] ISO 16770 – Plastics – Determination of environmental stress cracking (ESC) of
596 polyethylene – Full notch creep test (FNCT), 2004.
597 [19] ASTM D 5397 – Standard Test Method for Evaluation of Stress Crack Resistance of
598 Polyolefin Geomembranes Using Notched Constant Tensile Load Test, 2007.
599 [20] ASTM International. ASTM F1473-16 Standard Test Method for Notch Tensile Test to
600 Measure the Resistance to Slow Crack Growth of Polyethylene Pipes and Resins. West
601 Conshohocken, PA: ASTM International, 2016. Web. 31 Mar 2017.
602 [21] ASTM International. ASTM D1693-15 Standard Test Method for Environmental Stress-
603 Cracking of Ethylene Plastics. West Conshohocken, PA: ASTM International, 2015. Web. 31
604 Mar 2017.
605 [22] D. Huang, H. Zhou, L. Lin, Biodiesel: an Alternative to Conventional Fuel, Energy
606 Procedia. 16 (2012) 1874–1885. doi:10.1016/j.egypro.2012.01.287.
607 [23] E. Richaud, Flaconnèche Bruno, J. Verdu, Biodiesel permeability in polyethylene, Polymer
608 Testing. 31 (2012) 170–1076. doi:10.1063/1.4738433.
609 [24] M. Böhning, U. Niebergall, A. Adam, W. Stark, Influence of biodiesel sorption on
610 temperature-dependent impact properties of polyethylene, Polymer Testing. 40 (2014) 133–142.
611 doi:10.1016/j.polymertesting.2014.09.001.

612 [25] M.M. Maru, M.M. Lucchese, C. Legnani, W.G. Quirino, A. Balbo, I.B. Aranha, et al.,
613 Biodiesel compatibility with carbon steel and HDPE parts, Fuel Processing Technology. 90
614 (2009) 1175–1182. doi:10.1016/j.fuproc.2009.05.014.
615 [26] M. Böhning, U. Niebergall, A. Adam, W. Stark, Impact of biodiesel sorption on mechanical
616 properties of polyethylene, Polymer Testing. 34 (2013) 17–24.
617 doi:10.1016/j.polymertesting.2013.12.003.
618 [27] M. Böhning, U. Niebergall, M. Zanotto, V. Wachtendorf, Impact of biodiesel sorption on
619 tensile properties of PE-HD for container applications, Polymer Testing. 50 (2016) 315–324.
620 doi:10.1016/j.polymertesting.2016.01.025.
621 [28] M. Weltschev, J. Werner, M. Haufe, M. Heyer, Compatibility of High-Density Polyethylene
622 Grades with Biofuels, Packaging Technology and Science. 27 (2013) 231–240.
623 doi:10.1002/pts.2028.
624 [29] M. Thompson, B. Mu, C. Ewaschuk, Y. Cai, K. Oxby, J. Vlachopoulos, Long term storage
625 of biodiesel/petrol diesel blends in polyethylene fuel tanks, Fuel. 108 (2013) 771–779.
626 doi:10.1016/j.fuel.2013.02.040.
627 [30] A. Saad, F. Gomes, M. Thompson, Plasticizing effect of oxidized biodiesel on polyethylene
628 observed by nondestructive method, Fuel. 252 (2019) 246–253. doi:10.1016/j.fuel.2019.04.122.
629 [31] F. Gomes, W. West, M. Thompson, Effects of annealing and swelling to initial plastic
630 deformation of polyethylene probed by nonlinear ultrasonic guided waves, Polymer. 131 (2017)
631 160–168. doi:10.1016/j.polymer.2017.10.041.
632 [32] Y. Chen, Investigations of environmental stress cracking resistance of HDPE/EVA and
633 LDPE/EVA blends, Journal of Applied Polymer Science. 131 (2013). doi:10.1002/app.39880.

[33] A. Peterlin, Dependence of diffusive transport on morphology of crystalline polymers, Journal of Macromolecular Science, Part B. 11 (1975) 57–87. doi:10.1080/00222347508217855.

[34] A. Peterlin, Plastic deformation of polymers with fibrous structure, Colloid and Polymer Science. 253 (1975) 809–823. doi:10.1007/bf01452401.

[35] C.J. Lissenden, Y. Liu, G.W. Choi, X. Yao, Effect of Localized Microstructure Evolution on Higher Harmonic Generation of Guided Waves, Journal of Nondestructive Evaluation. 33 (2014) 178–186. doi:10.1007/s10921-014-0226-z.

[36] A. Lustiger, R. Markham, Importance of tie molecules in preventing polyethylene fracture under long-term loading conditions, Polymer. 24 (1983) 1647–1654. doi:10.1016/0032-3861(83)90187-8.

[37] R. Seguela, Critical review of the molecular topology of semicrystalline polymers: The origin and assessment of intercrystalline tie molecules and chain entanglements, Journal of Polymer Science Part B: Polymer Physics. 43 (2005) 1729–1748. doi:10.1002/polb.20414.

[38] G.Z. Voyiadjis, A. Shojaei, N. Mozaffari, Strain gradient plasticity for amorphous and crystalline polymers with application to micro- and nano-scale deformation analysis, Polymer. 55 (2014) 4182–4198. doi:10.1016/j.polymer.2014.06.015.

[39] C. Millot, R. Séguéla, O. Lame, L.-A. Fillot, C. Rochas, P. Sotta, Tensile Deformation of Bulk Polyamide 6 in the Preyield Strain Range. Micro–Macro Strain Relationships via in Situ SAXS and WAXS, Macromolecules. 50 (2017) 1541–1553. doi:10.1021/acs.macromol.6b02471.

[40] J. Cazenave, R. Seguela, B. Sixou, Y. Germain, Short-term mechanical and structural approaches for the evaluation of polyethylene stress crack resistance, Polymer. 47 (2006) 3904–3914. doi:10.1016/j.polymer.2006.03.094.

[41] L. Kurelec, M. Teeuwen, H. Schoffeleers, R. Deblieck, Strain hardening modulus as a measure of environmental stress crack resistance of high density polyethylene, Polymer. 46 (2005) 6369–6379. doi:10.1016/j.polymer.2005.05.061.

[42] A. Sharif, N. Mohammadi, S.R. Ghaffarian, Model prediction of the ESCR of semicrystalline polyethylene: Effects of melt cooling rate, Journal of Applied Polymer Science. 112 (2009) 3249–3256. doi:10.1002/app.29893.

[43] A. Krajenta, A. Rozanski, R. Idczak, Morphology and properties alterations in cavitating and non-cavitating high density polyethylene, Polymer. 103 (2016) 353–364. doi:10.1016/j.polymer.2016.09.068.

[44] C.J. Lissenden, Y. Liu, J.L. Rose, Use of non-linear ultrasonic guided waves for early damage detection, Insight - Non-Destructive Testing and Condition Monitoring. 57 (2015) 206–211. doi:10.1784/insi.2015.57.4.206.

[45] A.Y. Yarysheva, E.G. Rukhlya, L.M. Yarysheva, D.V. Bagrov, A.L. Volynskii, N.F. Bakeev, The structural evolution of high-density polyethylene during crazing in liquid medium, European Polymer Journal. 66 (2015) 458–469. doi:10.1016/j.eurpolymj.2015.03.003.

[46] M. Chan, J. Williams, Slow stable crack growth in high density polyethylenes, Polymer. 24 (1983) 234–244. doi:10.1016/0032-3861(83)90139-8.

[47] A. Lustiger, R.D. Corneliusen, The effect of an environmental stress cracking agent on interlamellar links in polyethylene, Journal of Polymer Science Part B: Polymer Physics. 24 (1986) 1625–1629. doi:10.1002/polb.1986.090240719.

[48] X. Lu, R. Qian, N. Brown, The effect of crystallinity on fracture and yielding of polyethylenes, Polymer. 36 (1995) 4239–4244. doi:10.1016/0032-3861(95)92219-5.

[49] A.N. Gent, Hypothetical mechanism of crazing in glassy plastics, Journal of Materials Science. 5 (1970) 925–932. doi:10.1007/bf00558171.

680 [50] G.A. Bernier, R.P. Kambour, The Role of Organic Agents in the Stress Crazing and Cracking of
681 Poly(2,6-dimethyl-1,4-phenylene oixde), Macromolecules. 1 (1968) 393–400.
682 doi:10.1021/ma60005a005.
683 [51] P. Hittmair, R. Ullman, Environmental stress cracking of polyethylene, Journal of Applied
684 Polymer Science. 6 (1962) 1–14. doi:10.1002/app.1962.070061901.
685 [52] P. Withers, H. Bhadeshia, Residual stress. Part 1 – Measurement techniques, Materials
686 Science and Technology. 17 (2001) 355–365. doi:10.1179/026708301101509980.
687 [53] P. Withers, H. Bhadeshia, Residual stress. Part 2 – Nature and origins, Materials Science
688 and Technology. 17 (2001) 366–375. doi:10.1179/026708301101510087.
689 [54] S. Daniewicz, An elastic-plastic analytical model for predicting fatigue crack growth in
690 arbitrary edge-cracked two-dimensional geometries with residual stress, International Journal of
691 Fatigue. 16 (1994) 123–133. doi:10.1016/0142-1123(94)90102-3.
692 [55] A. Lustiger, R.D. Corneliussen, The role of crazes in the crack growth of polyethylene,
693 Journal of Materials Science. 22 (1987) 2470–2476. doi:10.1007/bf01082132.
694 [56] J.J. Strebel, A. Moet, The effects of annealing on fatigue crack propagation in polyethylene,
695 Journal of Polymer Science Part B: Polymer Physics. 33 (1995) 1969–1984.
696 doi:10.1002/polb.1995.090331312.
697 [57] J. Runt, M. Jacq, Effect of crystalline morphology on fatigue crack propagation in
698 polyethylene, Journal of Materials Science. 24 (1989) 1421–1428. doi:10.1007/bf02397082.
699 [58] R. Bubeck, H. Baker, The influence of branch length on the deformation and microstructure
700 of polyethylene, Polymer. 23 (1982) 1680–1684. doi:10.1016/0032-3861(82)90193-8.
701 [59] J. Runt, K.P. Gallagher, The influence of microstructure on fatigue crack propagation in
702 polyoxymethylene, Journal of Materials Science. 26 (1991) 792–798. doi:10.1007/bf00588317.

[60] J.T. Yeh, J. Runt, Fatigue crack propagation in high-density polyethylene, Journal of Polymer Science Part B: Polymer Physics. 29 (1991) 371–388. doi:10.1002/polb.1991.090290313.

List of Figure:

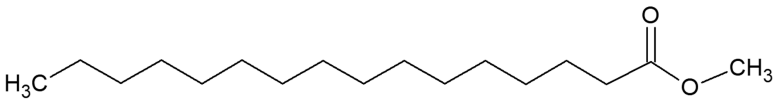

Figure 1. Generic chemical structure of biodiesel.

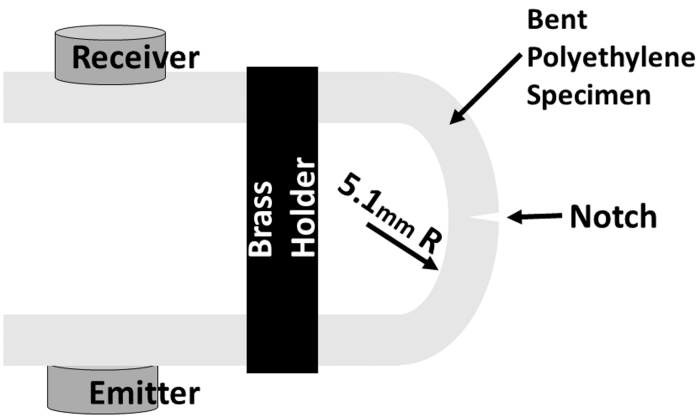

Figure 2. Conceptual drawing of a bent PE sample with the ultrasonic sensors coupled to the surface.

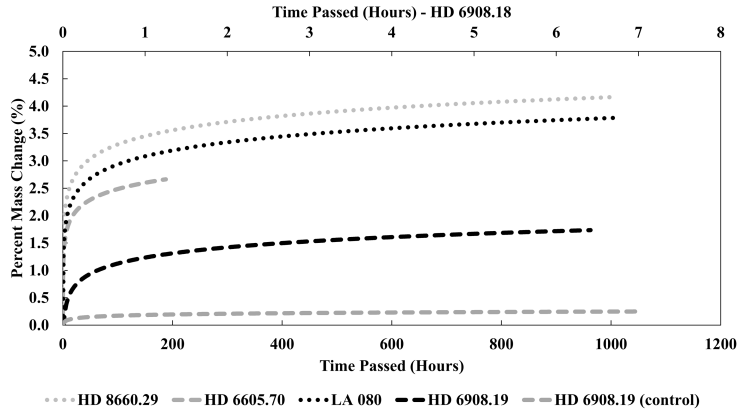

Figure 3. Plot of average percent weight change (%) vs. immersion time (hours) in 10% biodiesel for HD 8660.29 (gray dotted line), HD 6605.70 (gray dashed line), HD 6908.19 (black dashed line), and LA 080 samples (black dotted line). The control was run in water (gray dashed line).

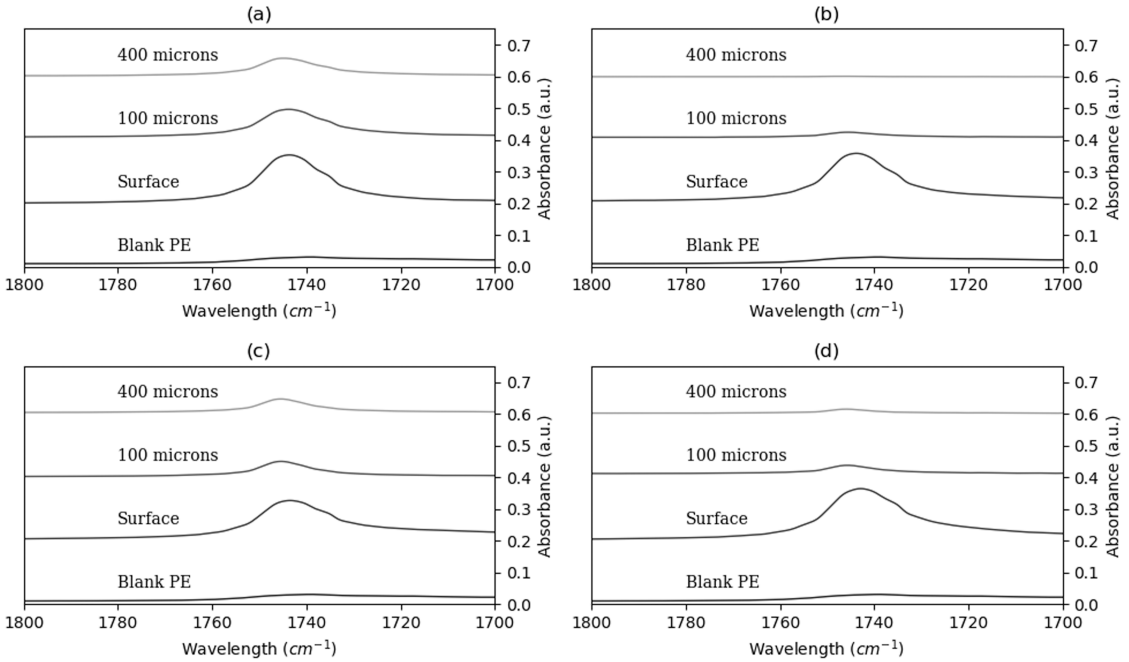

Figure 4. FT-IR (AT-R) spectra in the region of the ester group of biodiesel (1735-1750 cm^{-1}) for, a) (top left) HD 6605.70 – notch (crack); b) (top right) HD 6605.70 – specimen end; c) (bottom left) HD 8660.29 – notch; d) (bottom right) HD 8660.29 – specimen end. To allow better visualization of the changes, each spectrum attained was displaced by 0.2 above the preceding spectra.

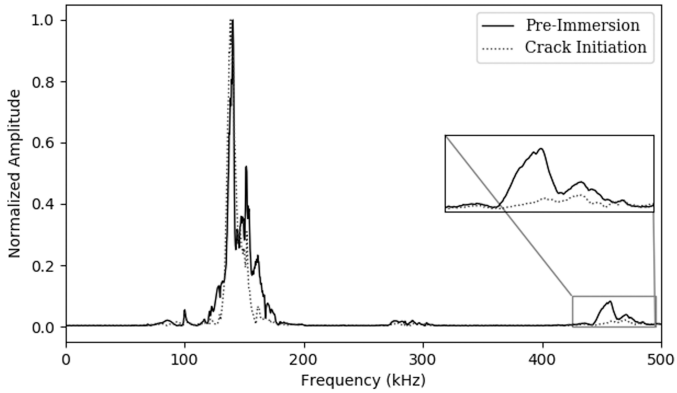

Figure 5. Ultrasonic spectra for the HD 6605.70 sample before testing and after cracking due to biodiesel immersion. The region highlighted in the box corresponded to the third harmonic region (A_3, between 400-500 kHz).

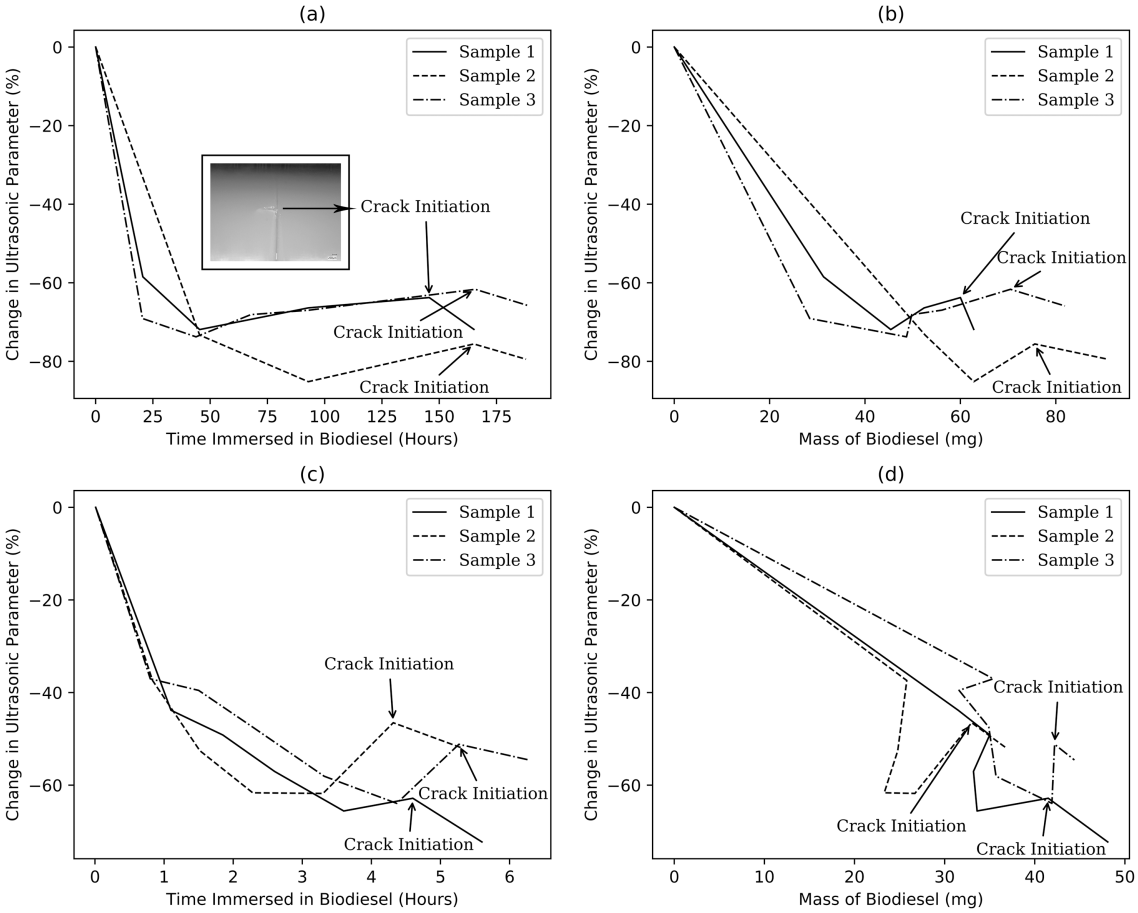

Figure 6. Variation in the nonlinear ultrasonic parameter versus (a) time of immersion in biodiesel or (b) mass of biodiesel absorbed, for HD 6605.70; and (c) time of immersion in biodiesel or (d) mass of biodiesel absorbed for HD 6908.19. Time at which cracking was first visually observed for each sample has been labelled as "crack initiation" on the plot and a microscope image of the initiated crack initiation in HD 6605.70 has been added.

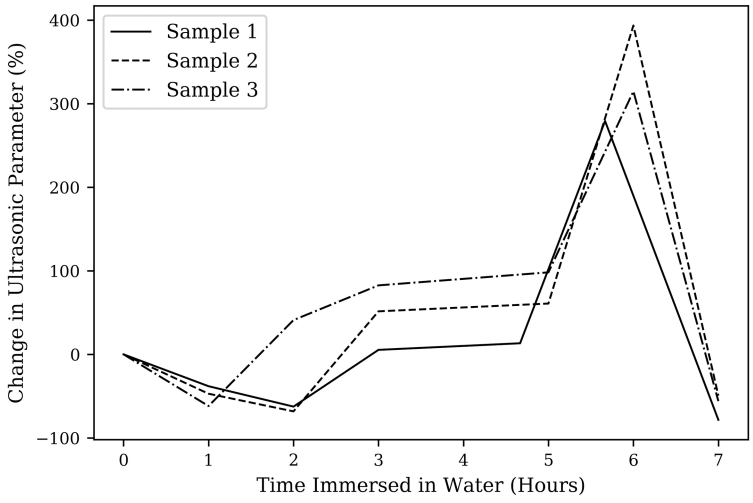

Figure 7. Variation in nonlinear ultrasonic parameter (%) vs time (Hours) for three HD 6908.19 samples immersed in water.

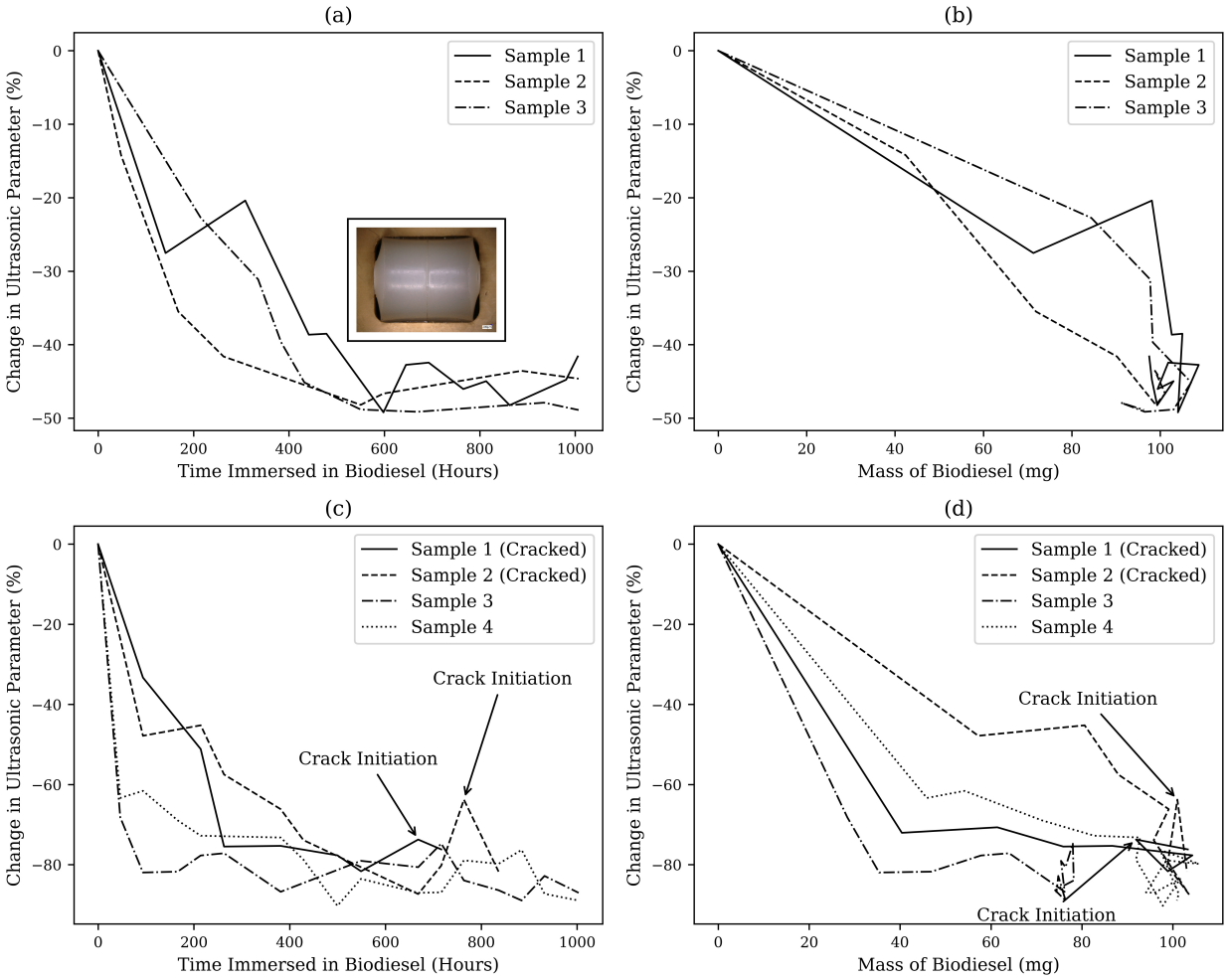

Figure 8. Variation in the nonlinear ultrasonic parameter versus (a) time of immersion in biodiesel or (b) mass of biodiesel absorbed, for HD 8660.29; and (c) time of immersion in biodiesel or (d) mass of biodiesel absorbed for LA 080. Time at which cracking was first visually observed for each sample that cracked has been labelled as "crack initiation" on the plot. Microscopic imaging of the notched area of Sample 1 of HD 8660.29 after >1000 hours of immersion in biodiesel has been added to the plot.

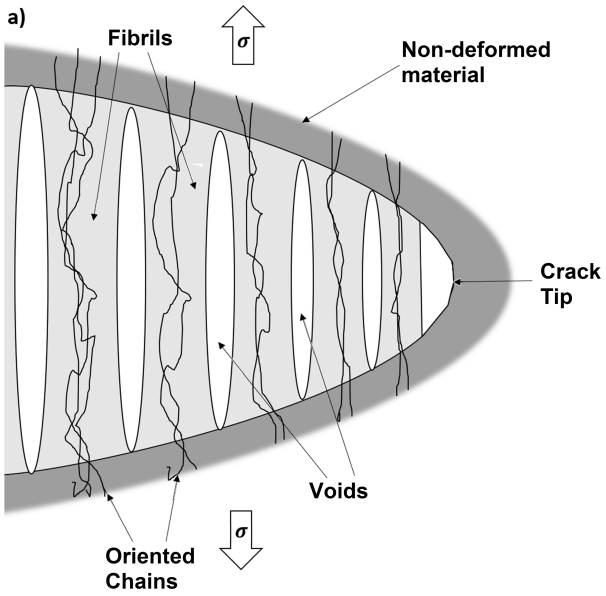

762

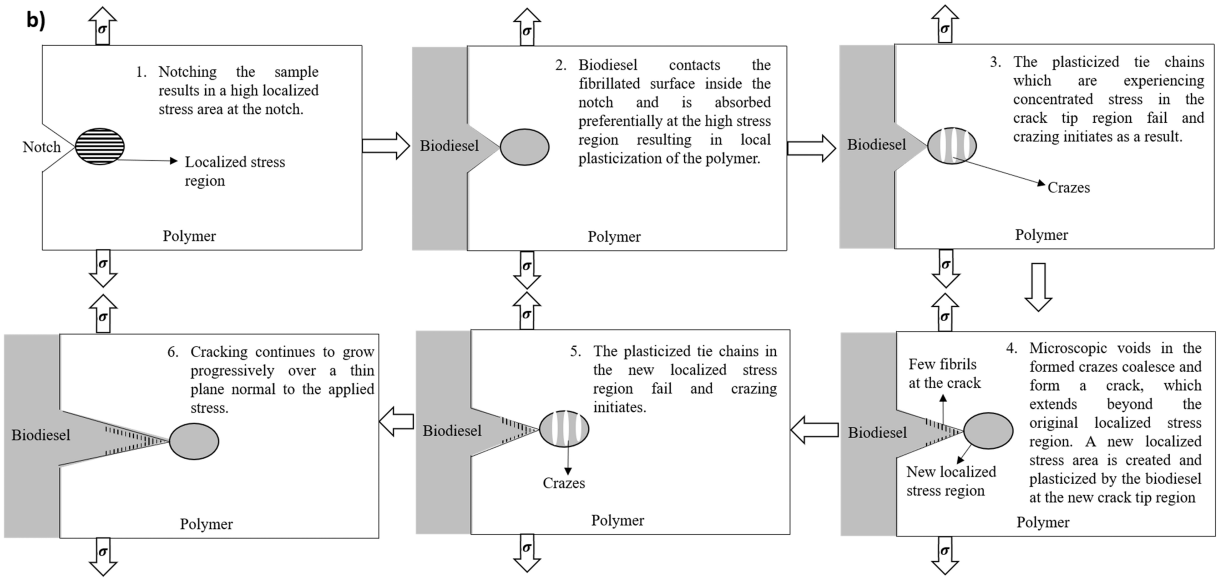

763

764 **Figure 9.** Conceptual drawing of ESC. (a) Fibrillated fracture occurring at the crack tip; (b)
765 mechanism of ESC of PE by biodiesel.

766

767

Table 1. Summary of key properties of all resins used in the experimental work.

Reference Code	Density (g/cm^3)	MFI (g/10min)	ESCR[1] (F_{50}hours, IGEPAL)
HD 6605.70	0.948	5.0	20
LA 080	0.954[2]	0.3[3]	47[4]
HD 8660.29	0.941	2.0	40
HD 6908.19	0.965	8.2	3

1) ESCR = environmental stress cracking resistance.
2) Density was measured using a Mirage MD-200S Electronic Densimeter. Three dog bone samples were used for average value quoted.
3) MFI = melt flow index, measured according to ASTM D1238.
4) Values were determined using ASTM D1693 with 10% IGEPAL CA-630.

Table 2. Summary of final mass change, ESCR (F_{50} hours) in biodiesel, and the estimated crystallinity values by DSC.

	PE Grade	Crystallinity (%)	Mass Change (%)	ESCR (F_{50}hours, biodiesel)
Uncracked Samples	**HD 8660.29**	50	4.17±0.15	>1000
	LA 080 - Uncracked	61	3.78±0.51	>1000
Cracked Samples	**HD 6605.70**	58	2.62±0.23	158.82±9.33
	LA 080 – Cracked	61	3.66±0.22	716.03±47.75
	HD 6908.19	69	1.65±0.26	4.73±0.40